

Quantitative Flow Visualization by Rainbow Schlieren Deflectometry and Pitot Pressure Measurements for Leek Peeler Nozzle Jets

Masatoshi Ezoe, Shinichiro Nakao, Yoshiaki Miyazato

Department of Mechanical Systems Engineering, The University of Kitakyushu, Fukuoka, Japan
Email: miyazato@kitakyu-u.ac.jp

How to cite this paper: Ezoe, M., Nakao, S. and Miyazato, Y. (2019) Quantitative Flow Visualization by Rainbow Schlieren Deflectometry and Pitot Pressure Measurements for Leek Peeler Nozzle Jets. *Journal of Flow Control, Measurement & Visualization*, 7, 44-60.
<https://doi.org/10.4236/jfcmv.2019.71004>

Received: October 19, 2018

Accepted: December 6, 2018

Published: January 23, 2019

Copyright © 2019 by author(s) and Scientific Research Publishing Inc.
This work is licensed under the Creative Commons Attribution International License (CC BY 4.0).
<http://creativecommons.org/licenses/by/4.0/>



Open Access

Abstract

To optimize the leek peeling performance, a new nozzle has been developed in which the nozzle has a design Mach number of 1.68, an inner diameter of 2.0 mm at the throat, and an inner diameter of 2.3 mm at the exit. Experiments have been conducted over a range of nozzle pressure ratios from 3.0 to 6.0. Flow field issued from the new nozzle is quantitatively visualized by the rainbow schlieren deflectometry and compared with that from a conventional nozzle. Density fields in the free jets are reconstructed by the Abel inversion method for the schlieren images with the horizontal rainbow filter. The density values at the exit of the conventional nozzle obtained by the rainbow schlieren are compared with the analytical results by the flow model proposed in the past. In addition, Pitot probe surveys along the jet centerline were made to obtain the impact pressure distributions. The Mach number and velocity distributions along the jet centerline are obtained from a combination of the density and Pitot pressure data to clarify the fundamental flow structure of leek peeler nozzle jets.

Keywords

Compressible Flow, Optical Observation, Leek Peeler Nozzle, Rainbow Schlieren Deflectometry, Pitot Pressure

1. Introduction

The average age of farmers of Japanese agriculture is 66.6 years old in 2017 [1] and aging is expected to accelerate rapidly year by year. It is obviously a daunting and time-consuming task for old farmers to peel white leeks before the shipment. Hence, in an agricultural sector in Japan, there are some cases to peel

leeks using the jet from a nozzle attached to a compressor which farmers generally hold as an air source. Air jets from leek peeler nozzles are often used to remove the outer layer of the leeks containing dirt as shown in **Figure 1** [2].

For the same nozzle and working distance, the peeling potential of leeks is conventionally presumed to be proportional to the stagnation pressure, just upstream of the nozzle. However, jet noises as well as fuel expenses required for working compressors increase with increasing nozzle operating pressure. To the authors' knowledge, leek peeler nozzle jets have never been studied so far from the viewpoint of fluid dynamics and there is no reliable data on leek peeler jets. Therefore, in the present study, two different nozzles for peeling white leeks are examined. One is a conventional nozzle with a cylindrical wall contour and the other is an improved nozzle with a convergent-divergent wall contour. The performance of leek peelers seems to depend on impact force of the jet. In industrial applications, Pitot pressure is regarded as a measure of impact force of a jet so that the efforts have been made to develop nozzles with a high Pitot pressure. However, a Pitot probe has limited spatial resolution and in supersonic flow the Pitot probe does not indicate the local total pressures, since a detached shock wave stands ahead of the tube. The detached shock also introduces disturbance or velocity change to the flow. Therefore, in addition to Pitot pressure measurements of jet flow fields, rainbow schlieren techniques [3] [4] are for the first time applied to the free jets issued from the conventional and improved nozzles for quantitative visualization of flow fields at high spatial resolution, and they will enable some progress in the understanding of the fundamental fluid dynamics of jets from leek peeler nozzles, since other properties of the jet flow fields including the Mach number, velocity, and temperature can be estimated from a combination of the density and Pitot pressure data. Although concerning the practical leek peeling process, jet inclined angles would have some effects on the peeling performance; the flow characteristics of free jets only are investigated as the first phase of the study.

2. Experimental Set-Up

2.1. Experimental Apparatus and Optical Systems

The experiments were performed in High-Speed Gasdynamics Research Laboratory at the University of Kitakyushu in Japan. **Figure 2** shows a schematic drawing of a blowdown type supersonic wind tunnel with simple optical configurations for the schlieren system.

The rectangular Cartesian coordinate system with the x , y , and z is also shown in **Figure 2**. The high-pressure dry air supplied by a compressor to an air storage tank is discharged into the atmosphere through a solenoid valve, a plenum chamber, and an axisymmetric supersonic nozzle. The air storage tank provides a total capacity of an approximate 2 m^3 and is capable of supplying air at a maximum storage pressure of 1 MPa. The solenoid valve is used to regulate the pressure in the plenum chamber, which can be held constant automatically

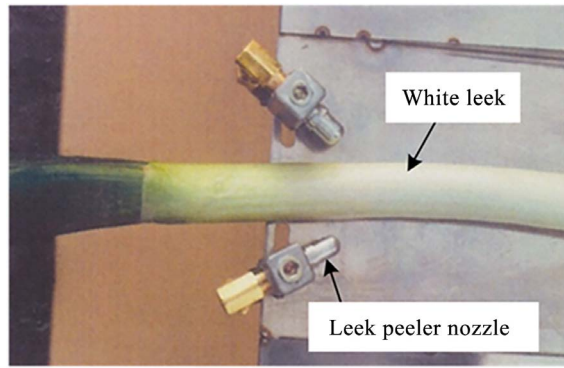


Figure 1. White leek on working bench with leek peeler nozzles.

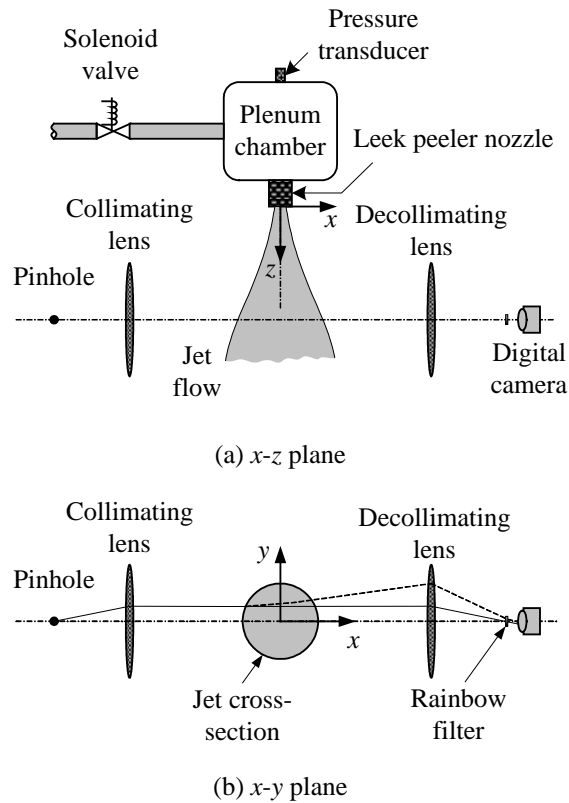


Figure 2. Experimental set-up with optical systems.

within ± 0.5 kPa as the plenum pressure varies. The temperature in the plenum chamber T_{os} is measured with a thermocouple, and it is maintained constant at ambient temperature T_b (approximately $298 \text{ K} \pm 0.1 \text{ K}$) during tests. The ambient density ρ_b and back pressure p_b are $1.18 \pm 0.05 \text{ kg/m}^3$ and $101 \pm 1 \text{ kPa}$, respectively.

The rainbow schlieren system shown in **Figure 2** consists of rail-mounted optical components including a 50 micron diameter pinhole, two 100 mm diameter, 500 mm focal length achromatic lenses, a computer generated 35 mm wide slide with color gradations in a 1.4 mm wide strip, and a digital camera with variable focal length lens. A continuous 250 W metal halide light source

connected to a 50 micron diameter fiber optic cable provides light inputs at the pinhole through a 16.56 mm focal length objective lens. The pinhole is placed at the focal point of the collimating lens to obtain collimated light rays. The camera output in the RGB format is digitized by a personal computer with 24 bit color frame grabber. As shown as the dashed line in **Figure 2(b)**, a light ray from the collimating lens is deflected while passing through the jet with refractive index gradients. The second lens decollimates the deflected ray to form a displaced image of the source at the cutoff plane. The camera lens is positioned beyond the rainbow filter and located to form an image of the jet flow onto the recorded medium of the digital camera. The rainbow filter is carefully adjusted for the light to be focused at a desirable hue on the filter.

The rainbow filter used in the present experiments is shown in **Figure 3**, and was fabricated in computer software and then printed digitally on a high resolution 35 mm color film recorder. It has continuous hue variation from $Hue = 0$ to 314 deg in a 1.4 mm wide strip and the origin $y = 0$ corresponds to $Hue = 185$ deg. The characteristics of the rainbow filter were obtained by traversing the filter in intervals of 0.1 mm in the y direction at the cutoff plane of the rainbow schlieren apparatus in **Figure 2** before starting experiments. The reconstruction of density fields from rainbow schlieren pictures was performed using the Abel inversion technique, which is effective for axisymmetric flows. Detailed description of the rainbow filter calibration and the method for determining the density field in an axisymmetric jet from experimental schlieren images are given in the paper by Al-Amar *et al.* [3].

2.2. Leek Peeler Nozzles

A schematic drawing of a conventional leek peeler nozzle is shown in **Figure 4**. It has a cylindrical internal wall contour with an inner diameter of 2.0 mm and a longitudinal length of 25 mm, and it has a square corner at the nozzle inlet and exit. A new leek peeler nozzle shown in **Figure 5** was fabricated by Meiji Air Compressor MFG. Co., Ltd., Okayama, Japan, and the improved nozzle has an inner diameter of 2.0 mm at the throat and an inner diameter of 2.3 mm at the exit. The nozzle manufacturing method used in the present study is representative of the design of practical leek peeler nozzles. Such nozzles do not have smoothly varying contours designed by the method of characteristics to produce shock-free jets in the design condition, and instead, they have a conical converging section, a constant-area throat, and a conical diverging section followed by a short straight section which will have a simple structure for mass-producing. The method of characteristics is not appropriate for nozzles with small diameters used in the present study.

The jet from the improved nozzle is expected to be correctly expanded for a nozzle pressure ratio of 4.8 when the nozzle flow obeys the isentropic process and then a Mach number of 1.68 at the nozzle exit. The inviscid theory shows that the flow through the improved nozzle are categorized into three different jet

flow fields: the flow with a stationary normal shock in the divergent portion of the nozzle for a range of nozzle pressure ratios from 1.2 to 1.5, overexpanded free jet for a range of pressure ratios between 1.5 and 4.8, and underexpanded free jet for pressure ratios beyond 4.8.

2.3. Pitot Probe

The jet flow field has been measured also by a conventional Pitot probe as shown in Figure 6. The tip of the probe has an outer diameter of 0.81 mm, an inner diameter of 0.51 mm, and a tip length of 20 mm. The outside hole of the Pitot probe was connected to one side of a Toyoda semiconductor pressure transducer (Model PMS-5-1M). The Pitot probe was mounted on a two-dimensional traversing device to scan the flow field and Pitot pressure measurements were made at intervals of 1.0 mm along the nozzle axis from $z = 0$ mm to 50 mm and they were based on continuous sampling while moving the probe along the nozzle axis, allowing enough time to reach steady state at each measuring location. The average value at each location was computed from 100 samples taken at 1 kHz and a similar measurement was repeated at least 5 times for the same nozzle pressure ratio to obtain the precision errors for the measurements.

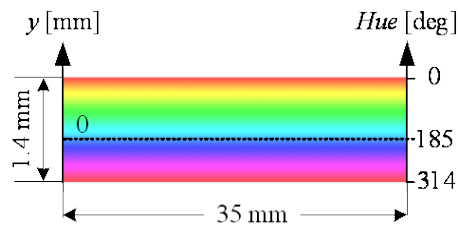


Figure 3. Rainbow filter.

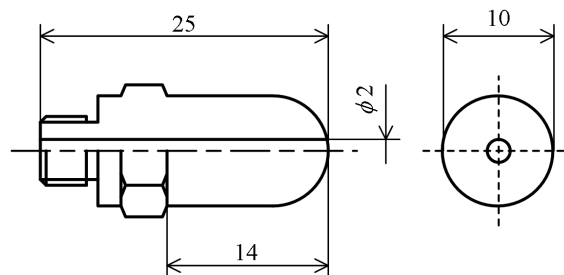


Figure 4. Conventional leak peeler nozzle (dimensions in mm).

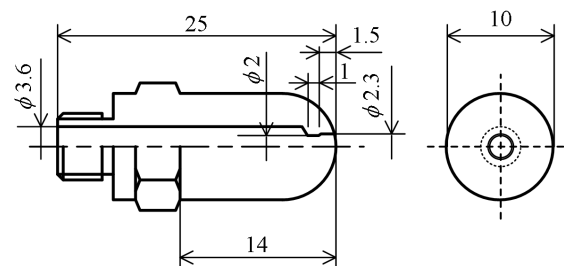


Figure 5. Improved leak peeler nozzle (dimensions in mm).

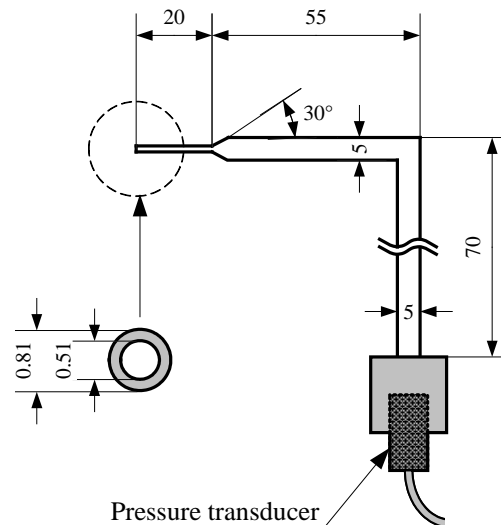


Figure 6. Schematic drawing of Pitot probe (dimensions in mm).

3. Results and Discussion

3.1. Rainbow Schlieren Pictures

The rainbow filter shown in Figure 3 was used to visualize the jets from conventional and improved nozzle. The free jets for four nozzle pressure ratios of NPR ($=p_{os}/p_b$) = 3.0, 4.0, 5.0, and 6.0 are displayed with the rainbow schlieren visualization where the back pressure p_b is the same as the atmospheric pressure and plenum pressure p_{os} only is varied by adjusting the solenoid valve.

The rainbow schlieren pictures for free jets from the conventional nozzle are presented in Figure 7 and Figure 8 with flow from left to right. Figure 7 shows schlieren pictures with the horizontal rainbow filter and the filter is set in the same orientation as in Figure 3. Also, Figure 8 shows schlieren pictures with the vertical rainbow filter and the filter is set by turning it 90 degrees counterclockwise. When NPR is held constant at 3.0 as shown in Figure 7(a) and Figure 8(a), the jet boundary from the nozzle exit diverges slightly. Hence, the jet flow is underexpanded with a regular and quasi-periodic shock cell structure extending over z equaling about 17 mm. The streamwise distances from the nozzle exit for typical shock cells in the free jets are shown in Figure 8(b) with the symbol (① - ④) having an upward arrow for each shock cell. In case of $NPR = 4.0$ (Figure 8(a) and Figure 8(b)), the number of shock-cells, the spacing between respective shock-cells in the jet flow and the overall length of the shock-cell structure increase as compared with the case for $NPR = 3.0$.

As shown in Figure 7(c) and Figure 8(c), an increase of NPR from 4.0 to 5.0 makes the first shock-cell extremely strong and a Mach disk with 0.42 mm in diameter appears at z equaling about 2.5 mm. However, the subsequent shock cells hold the regular and quasi-periodic structure. As seen in Figure 7(d) and Figure 8(d), further increase of NPR to 6.0 causes the Mach disk to shift slightly downstream by 0.2 mm with its diameter increased to 0.78 mm and the first shock in the shock cell structure becomes particularly strong. It is quite likely

that jets with a Mach disk are responsible for intense shock-associated noise consisting of the screech tones and the broadband shock-associated noise [5], because the intensity of broadband shock-associated noise depends critically on the strength of the shocks in the shock-cell structure.

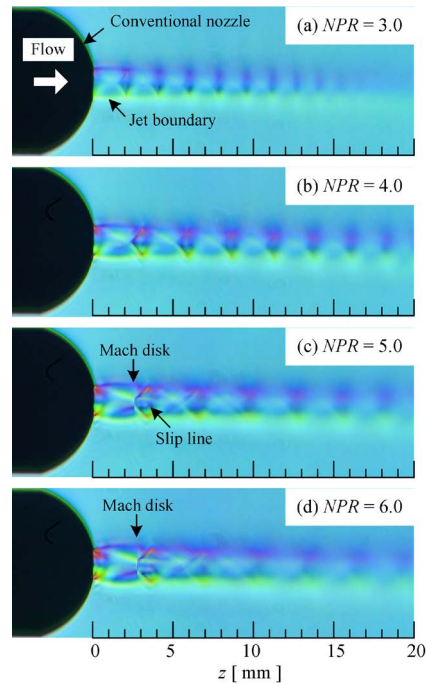


Figure 7. Schlieren pictures with horizontal rainbow filter for conventional nozzle.

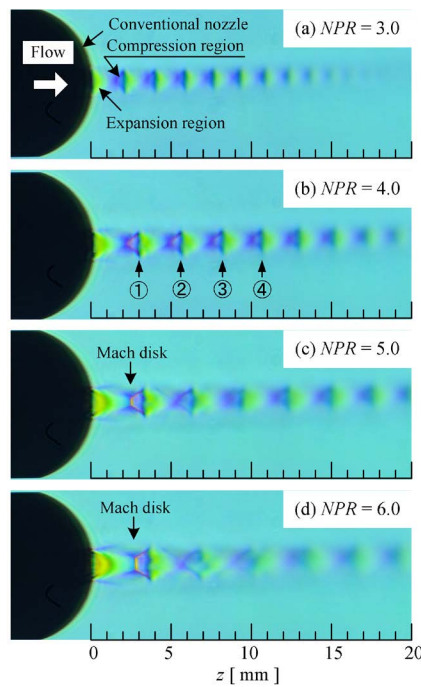


Figure 8. Schlieren pictures with vertical rainbow filter for conventional nozzle.

Typical rainbow schlieren pictures of the jets from the improved nozzle are presented in **Figure 9** and **Figure 10** corresponding to **Figure 7** and **Figure 8**, respectively, for the conventional nozzle. As mentioned previously, the improved nozzle jet is overexpanded for $NPRs = 3.0$ and 4.0 by the calculation based upon the one-dimensional inviscid theory. As a result, in case of **Figure 9(a)** for $NPR = 3.0$, no distinct shock-cell structure appears in the jet from the nozzle exit plane, and **Figure 10(a)** for the same nozzle pressure ratio shows a shock wave just downstream of the nozzle exit plane. The shock wave can be considered to be an oblique shock wave with a Mach disk.

As shown in **Figure 9(b)** and **Figure 10(b)**, when NPR increases from 3.0 to 4.0 , the oblique shock is weaker in its strength when compared with those in **Figure 9(a)** and **Figure 10(a)**, and the nozzle outflow is supersonic and a succession of two-dimensional oblique shocks and expansion waves appear inside the jet flow. For $NPR = 5.0$, the nozzle is almost correctly expanded as shown in **Figure 9(c)** and **Figure 10(c)**. Consequently, the shock disappears and the flow is supersonic with weak Mach waves in the jet flow. Schlieren pictures in **Figure 9(d)** and **Figure 10(d)** for $NPR = 6.0$ show that the nozzle is slightly underexpanded and a Mach disk cannot be seen in these pictures.

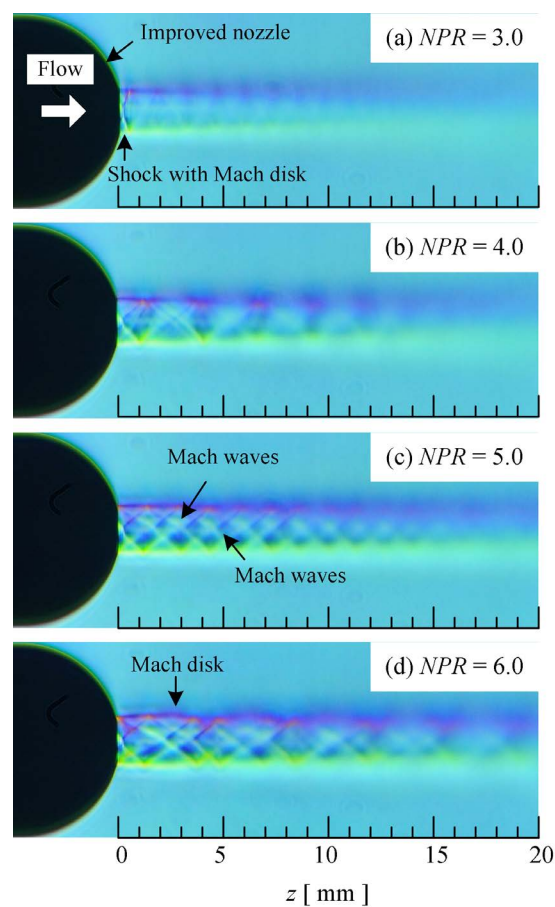


Figure 9. Schlieren pictures with horizontal rainbow filter for improved nozzle.

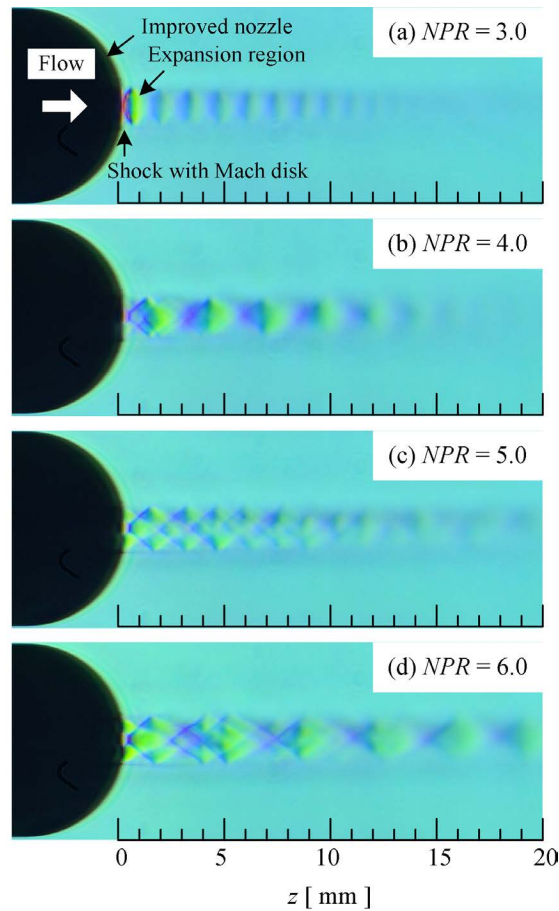


Figure 10. Schlieren pictures with vertical rainbow filter for improved nozzle.

In general, mass flow rates through nozzles with high pressure ratios depend only on the plenum pressure upstream of the nozzle and the area at the nozzle throat (the area at the nozzle exit for the conventional nozzle). The improved nozzle has the same throat area as the conventional nozzle, and therefore, both nozzles have the same air consumption rate. Furthermore, the dominant noise issued from free jets with high pressure ratios are shock-associated noises which are produced as a result of an interaction between shock waves and jet shear layers. The free jets issued from the improved nozzle contain weak shock waves when compared with those from the conventional nozzle for the practical operating condition ($NPRs = 5$ and 6) in leak peering process. Thus, the improved nozzle would be more effective for noise reduction compared with the conventional nozzle.

3.2. Density Distributions along Jet Centerline

A comparison of centerline density distributions of the free jets from the conventional and improved nozzles is presented in **Figure 11**. The abscissa indicates the downstream distance z [mm] from the nozzle exit plane and the ordinate denotes the local density of the jet. The red and blue lines show the results for

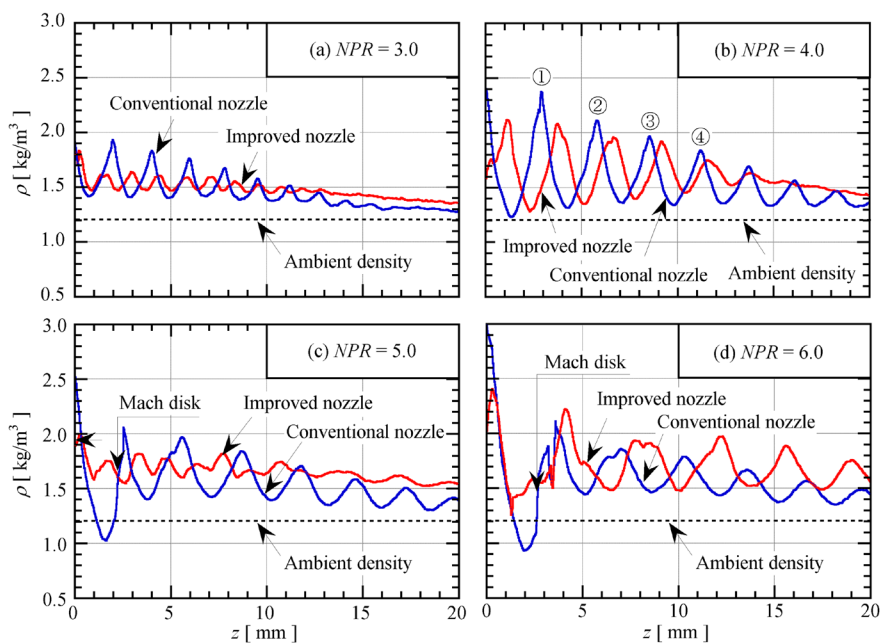


Figure 11. Centerline density distributions for conventional and improved nozzles.

the improved and conventional nozzle, respectively, and the black line is the ambient density $\rho_b = 1.18 \text{ kg/m}^3$.

Figure 11(a) shows that the jet from the conventional nozzle is underexpanded with a wavy form due to the regular and quasi-periodic shock-cell structure. On the other hand, the jet from the improved nozzle is overexpanded with a strong shock wave immediately downstream of the nozzle exit where the shock extends across both of the regions of the inside and outside of the nozzle exit as it can be imperceptibly seen in the schlieren picture of **Figure 10(a)** and the strength of each shock cell is weaker than that for the jet issued from the conventional nozzle. As shown in **Figures 11(b)-(d)**, the free jets from the conventional nozzle gets around to producing a strong oblique shock (symbols ① - ④ in **Figure 11(b)**) or a Mach disk (**Figure 11(c)** and **Figure 11(d)**) as the degree of expansion increases, but an increase of NPR from 3.0 to 5.0 for the improved nozzle changes the flow characteristic from the overexpansion to nearly correct expansion and it causes the strength of the shock-cell to attenuate. In addition, the jet from the improved nozzle shows a slightly wavy form on the centerline density distribution due to the Mach waves in the jet flow and keeps almost the same density value over the distance far downstream of the nozzle exit. In the case of $NPR = 6.0$, the jet from the improved nozzle becomes an underexpanded state. As a result, slightly strong shocks appear in the shock-cell again.

We consider the density value at the nozzle exit plane for $NPR = 5.0$ in **Figure 11(c)**, since leek peeler nozzle jets are often used at working pressure ratios between $NPR = 5.0$ and 6.0. The one-dimensional isentropic theory for the improved nozzle shows a density value of 1.93 at the nozzle exit plane. Good quan-

titative agreement can be seen from a comparison between the theory and experiment. On the other hand, when the flow through the conventional nozzle is assumed to be isentropic, the density value at the nozzle exit plane becomes 3.74 and the corresponding experimental density value is 2.52, which is considerably lower than the theoretical one. This means that the losses including wall frictions as well as shock waves exist inside the conventional nozzle, for the flow in the contractions at the nozzle inlet may be choked [6], hence, it can be inferred that a shock wave stands at a position inside the nozzle. To clarify the cause of flow losses in the conventional nozzle, the present experimental data from the rainbow schlieren in **Figure 11** are quantitatively compared with the analytical results estimated using the flow model proposed by Nakajima *et al.* [7]. A comparison of the experiment, analysis, and theory for the density value at the nozzle exit are shown in **Figure 12**.

The flow model of Nakajima *et al.* assumes that an incoming flow through a constant-area long pipe with the sharp corners at the nozzle inlet and exit produces a normal shock due to an effect of the vena contracta just downstream of the nozzle inlet before being choked at the nozzle exit due to the wall friction. As shown in **Figure 12**, the densities at the nozzle exit calculated by one-dimensional theory and the flow model is directly proportional to *NPR* and for higher *NPRs*, the experimental data are in good quantitative agreement with the flow model of Nakajima *et al.*, which means that the flow in the conventional nozzle contains shock loss as well as friction loss for higher *NPRs*.

3.3. Pitot Pressure Distributions along Jet Centerline

Pitot probe surveys of free jets issued from the conventional and improved nozzles were made to obtain the impact pressure on the jet centerline over a range of four nozzle pressure ratios (*NPRs* = 3.0, 4.0, 5.0, and 6.0), and the results are plotted in **Figure 13** against the streamwise distance z where the ordinate denotes the Pitot pressure p_i [kPa]. The Pitot pressure is defined as the pressure measured by a Pitot probe aimed directly against the flow direction. Therefore, when the local flow speed is supersonic, the Pitot pressure includes total pressure loss caused by a standing bow shock in front of the Pitot probe. The peeling potential of the jet is conventionally presumed to be correlated with the Pitot pressure. The Pitot pressures at $z = 0$ for the conventional nozzle almost coincide with the plenum pressure p_{os} for each experimental condition, for the tip (0.81 mm in diameter) of the Pitot probe entirely plugs the exit (2.0 mm in diameter) of the nozzle except for a small leak, but those for the improved nozzle do not accord with the plenum pressures due to the larger nozzle diameter (2.3 mm).

As shown in **Figure 13** for the smallest pressure ratio, the Pitot pressure for the conventional nozzle is kept almost constant with small spatial fluctuations due to the shock-cell structure of the jet over the streamwise distance from the nozzle exit to z equaling around 10 mm and then gradually decreases toward

downstream. On the other hand, the Pitot pressure for the improved nozzle gradually increases over a range of distances from $z = 0$ to around 10 mm and it remains almost kept constant between z equaling around 10 mm and 15 mm and then gradually decreases toward downstream. The Pitot impact pressure for the conventional nozzle is always higher than that for the improved nozzle over the whole region measured. In the case of $NPR = 4.0$ (Figure 13(b)), the Pitot pressure for the conventional nozzle matures into a periodical wave with a large amplitude when compared with that in the case of $NPR = 3.0$. The Pitot pressure for the improved nozzle is kept almost constant from the nozzle exit to the z equaling around 10 mm and then gradually decreases, yet still lower than that for the conventional nozzle.

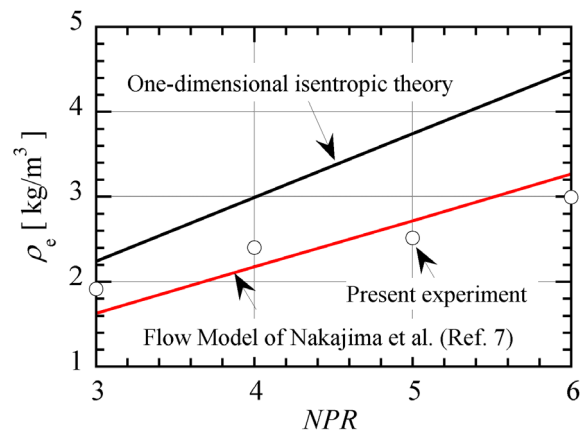


Figure 12. Comparison of theory with exit density of conventional nozzle.

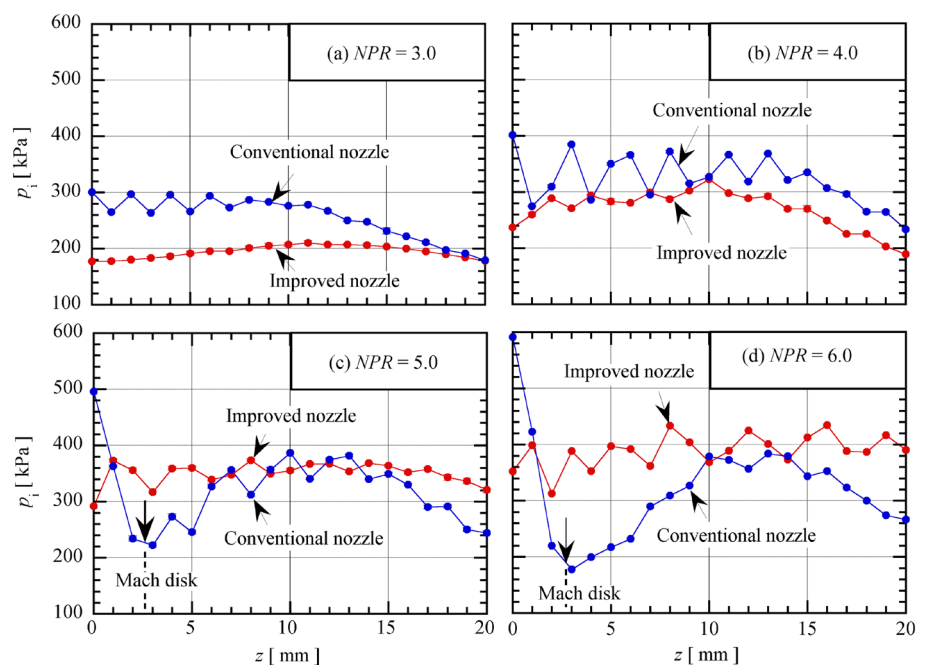


Figure 13. Centerline Pitot pressure distributions for conventional and improved nozzles.

The downward arrow on the Pitot pressure distribution for the conventional nozzle in **Figure 13(c)** and **Figure 13(d)** indicates the Mach disk location obtained from the rainbow schlieren picture and these figures show that the Pitot impact pressure decreases rapidly from the nozzle exit to the Mach disk due to the expansion waves from the nozzle lip and then gradually increases after the Mach disk. A similar phenomenon relating to the recovery of the Pitot pressure behind the Mach disk was reported also by Donaldson *et al.* [8], Samimy *et al.* [9] and Katanoda *et al.* [10]. To clarify the Pitot pressure recovery after a Mach disk, numerical simulation using the Euler equations was made by Katanoda *et al.* [10], who showed that the Pitot pressure remains almost constant downstream of the Mach disk and found a large discrepancy between experiment and simulation. Katanoda *et al.* [10] [11] presumed that the Pitot pressure recovery is attributed to the transfer of momentum from the region outside the slip streams formed by the triple point of the Mach disk to the central part of the jet. However, the detailed mechanism of Pitot pressure recovery is still controversial and further studies are required to grapple with the phenomenon.

Figure 13(c) shows that the Pitot pressure is kept almost constant over a whole region, for the jet flow is nearly correctly expanded. The Pitot pressure for the improved nozzle is higher than that for the conventional nozzle at the regions across the Mach disk and far downstream. As shown in **Figure 13(d)** for $NPR = 6.0$, the improved nozzle is slightly underexpanded and the jet contains the shock-cell structures over the regions far downstream of the nozzle exit. Nevertheless, the Pitot pressure is in total higher for improved nozzle than the conventional one except for the regions just behind the nozzle exit and over a range from $z = 10$ mm to 15 mm, for the jet from the improved nozzle includes negligible loss as compared with that from the conventional nozzle and in particular the jet from the improve nozzle does not contain a Mach disk.

3.4. Mach Number and Velocity Distributions along Jet Centerline

The Pitot pressure and density data are available to calculate the Mach number distributions along the jet centerline. Considering that Pitot pressures contain the normal shock loss when the flow Mach number M is greater than 1, a combination of the Pitot pressure p_i and density ρ leads to

$$\frac{p_i}{\rho} = \frac{\left(\frac{\gamma+1}{2} M^2\right)^{\frac{\gamma}{\gamma-1}}}{1 + \frac{\gamma+1}{2} M^2} \left(\frac{\gamma+1}{2\gamma M^2 + 1 - \gamma}\right)^{\frac{1}{\gamma-1}} RT_b \quad \text{for } M > 1 \quad (1)$$

and for flow Mach numbers less than or equal to 1,

$$M = \sqrt{\frac{2}{\gamma-1} \left[\left(\frac{p_i}{\rho RT_b}\right)^{\gamma-1} - 1 \right]} \quad \text{for } M \leq 1 \quad (2)$$

where $\gamma = 1.4$ is the specific heat ratio, $R = 287$ J/(Kg·K) is the gas constant, and $T_b = 298$ K is the ambient temperature.

The Mach number distributions along the jet centerline obtained using Equations (1) and (2) are shown in **Figure 14**. **Figure 14(a)** shows that the free jet issued from the conventional nozzle remains supersonic over the entire range downstream of the nozzle exit and its Mach number distribution contains wave undulation due to weak shocks just downstream of the nozzle exit. On the other hand, the free jet issued from the improved nozzle is subsonic just downstream of the nozzle exit and gradually increases in the downstream direction, and it reaches a Mach number of 1 and almost the same state is maintained. As shown in **Figure 14(b)**, the Mach number distributions for conventional and improved nozzles in case of $NPR = 4.0$ display a variation similar to each other in which both of the distributions contain wave forms responsible for the shock cell structure. For $NPRs = 5.0$ and 6.0 , the free jet issued from the improved nozzle almost keeps the design Mach number 1.68. The free jet from the conventional nozzle exhibits a noticeable variation contributing to a Mach disk just behind of the nozzle exit followed by strong shocks in the shock cell structure. The reason why the flow just downstream of the Mach disk is not subsonic for $NPR = 5.0$ is that the Pitot tube used in the present study has a large outer diameter (0.81 mm) compared with the diameter (0.42 mm) of the Mach disk, and, the Pitot measurement does not capture the Mach disk precisely.

Flow velocities are of particular significance for leek peeling process. A Mach number is not directly proportional to the corresponding flow velocity because it is a function of flow velocity and sound velocity. The flow velocity V can be calculated based on the appropriate assumption that the flow field of the free jet is adiabatic, *i.e.*

$$V = M \sqrt{\frac{1 + \frac{\gamma - 1}{2} M^2}{\gamma RT_b}} \quad (3)$$

Substitution of the Mach number of Equations (1) or (2) into Equation (3) leads to the velocity distributions along the jet centerline, and the result obtained are given in **Figure 15**.

Centerline velocity distributions in **Figure 15** show a similar trend as the corresponding Mach number distributions in **Figure 14**, for the flow velocity V varies linearly against the Mach number M in the case of adiabatic flow. As shown in **Figure 15(d)**, it is found that for the free jet issued from the conventional nozzle the Mach disk causes the flow velocity to fall abruptly from around 500 m/s to 200 m/s.

4. Concluding Remarks

Two different nozzles for peeling white leeks were examined in the present study. One was a conventional nozzle with a cylindrical wall contour and the other was an improved nozzle with a convergent-divergent wall contour. The rainbow schlieren visualization and Pitot pressure surveys were made for the jet from each nozzle. It was found that the jets from the conventional nozzle are

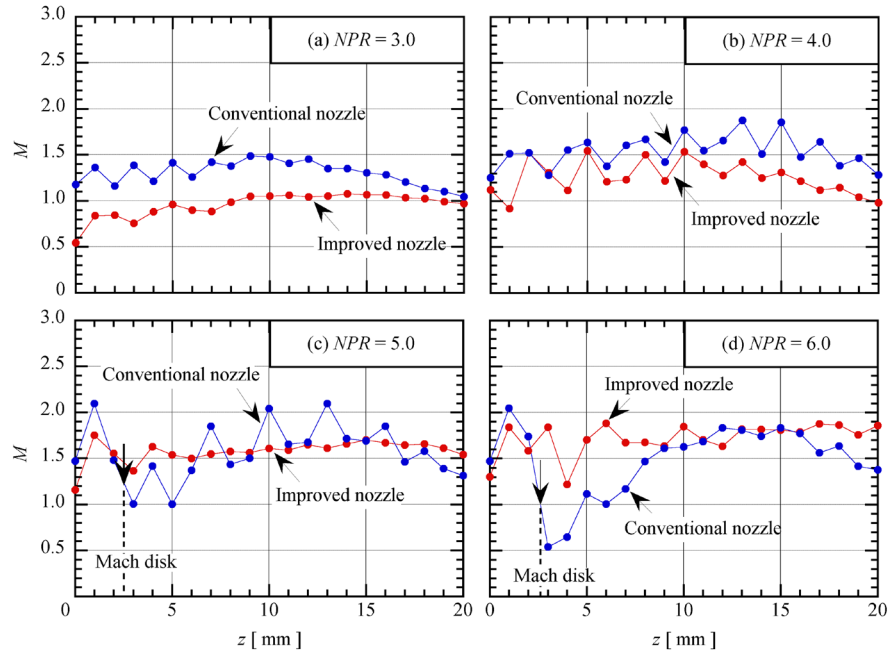


Figure 14. Centerline Mach number distributions for conventional and improved nozzles.

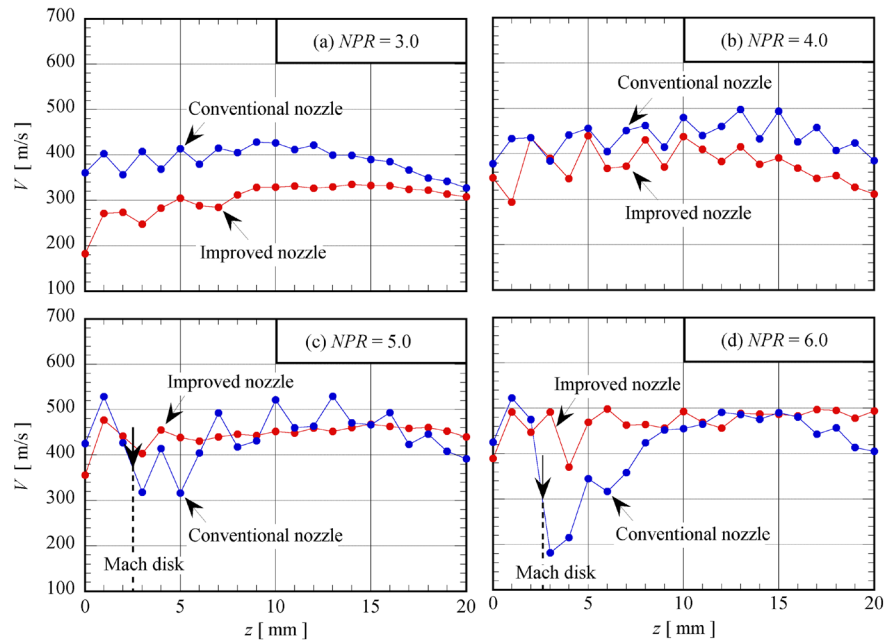


Figure 15. Centerline flow velocity distributions for conventional and improved nozzles.

underexpanded over a range of nozzle pressure ratios from $NPR = 3.0$ to 6.0 and contain a typical shock-cell structure for the full range of nozzle pressure ratios studied. In particular, for working pressure ratios of $NPR = 5.0$ and 6.0 , a Mach disk appears just downstream of the nozzle exit and it causes a significant pressure loss. On the other hand, the jets from the improved nozzle show an overexpanded state for NPR s of 3.0 and 4.0 , nearly correctly expanded state for $NPR =$

5.0, and underexpanded state for $NPR = 6.0$. For working pressure ratios range of $NPR = 5.0$ to 6.0 , jets from the improved nozzle can get higher working efficiency than the conventional one. The densities at the exit of the conventional nozzle were compared with the analytical values by the flow model proposed in the past and it was found that the flow in the conventional nozzle contains shock loss as well as friction loss for higher $NPRs$. The improved nozzle developed in the present study will be very valuable to the older farmers in agriculture. It was also found that the jet from the improved nozzle has higher removing potential for peeling leeks in comparison with the conventional one.

The Mach number and velocity distributions along the jet centerline were obtained from a combination of the Pitot pressure and density data and a quantitative comparison between free jet fields issued from the conventional and improved nozzles was made to demonstrate the fundamental characteristics of both the flow fields from a fluid dynamic point of view. The Pitot pressure, density, Mach number and velocity data presented here are considered to be of suitable quantity and quality that they form an appropriate database to act as a CFD validation test case in the future, and, the authors believe that the data will be effective for the design of more efficient leek peeler nozzles.

Acknowledgements

The authors would like to gratefully acknowledge the assistance of graduate students Takayuki Kunimasa and Kodai Azuma of the University of Kitakyushu during the terms in preparing and carrying out the present experiments. Special thanks go also to Kazuhiko Yoshino of Meiji Air Compressor MFG. Co., Ltd. for providing the leek peeler nozzles. Finally, the authors are grateful to Dr. Zensho Nakao (Professor Emeritus, University of the Ryukyus) for a careful review as well as suggestions for improving the manuscript.

Conflicts of Interest

The authors declare no conflicts of interest regarding the publication of this paper.

References

- [1] In Japanese. <http://www.maff.go.jp/j/tokei/sihyo/data/08.html>
- [2] (2012) The Sanyo Shinbun, 29. (In Japanese)
- [3] Al-Ammer, K.K., *et al.* (1998) Application of Rainbow Schlieren Deflectometry for Concentration Measurements in an Axisymmetric Helium Jet. *Experiments in Fluids*, **25**, 89-95.
- [4] Maeda, S., Fukuda, H., Kubo, K., Nakao, S., Ono, D. and Miyazato, Y. (2018) Structure of Underexpanded Supersonic Jets from Axisymmetric Laval Nozzles. *Journal of Flow Visualization and Image Processing*, **25**, 33-46.
- [5] Tam, C.K.W. (1995) Supersonic Jet Noise. *Annual Review of Fluid Mechanics*, **27**, 17-43. <https://doi.org/10.1146/annurev.fl.27.010195.000313>
- [6] Marjanovi, Ć.P. and Djordjevi, Ć.V. (1994) On the Compressible Flow Losses

- Through Abrupt Enlargements and Contractions. *Journal of Fluids Engineering*, **116**, 756-762.
- [7] Nakajima, R., Konishi, K., Oka, T., Ono, D. and Miyazato, Y. (2014) Density Measurements in Cylindrical Nozzle Jets by Rainbow Schlieren Deflectometry. *JSASS*, **12**, a133-a140.
- [8] Donaldson, C.D. and Snedeker, R.S. (1971) A Study of Free Jet Impingement, Part 1. Mean Properties of Free and Impinging Jets. *Journal of Fluid Mechanics*, **45**, 281-324. <https://doi.org/10.1017/S0022112071000053>
- [9] Samimy, M., Zaman, K.B.M.Q. and Reeder, M.E. (1993) Effect of Tabs on the Flow and Noise Field of an Axisymmetric Jet. *AIAA Journal*, **31**, 609-619. <https://doi.org/10.2514/3.11594>
- [10] Katanoda, H., Miyazato, Y., Masuda, M. and Matsuo, K. (2000) Pitot Pressures of Correctly-Expanded and Underexpanded Free Jets from Axisymmetric Supersonic Nozzles. *Shock Waves*, **10**, 95-101. <https://doi.org/10.1007/s001930050182>
- [11] Katanoda, H., Handa, T., Miyazato, Y., Masuda, M. and Matsuo, K. (2001) Effect of Reynolds Number on Pitot-Pressure Distributions in Underexpanded Supersonic Freejets. *Journal of Propulsion and Power*, **17**, 940-942.

Nomenclature

Hue: Hue [deg]

M: Mach number [-]

NPR: Nozzle pressure ratio [= p_{os}/p_b]

p_{os} : Plenum pressure [Pa]

p_b : Back pressure [Pa]

p_i : Pitot pressure [Pa]

R: Gas constant [J/(kg K)]

T_{os} : Temperature in plenum chamber [K]

T_b : Ambient temperature [K]

V: Flow velocity [m/s]

x, y, z: Rectangular Cartesian coordinate system

γ : Specific heat ratio [-]

ρ : Density [kg/m³]

ρ_b : Ambient density [kg/m³]

ρ_e : Density [kg/m³]